Effects of partial substitution by 5*d* heavy elements on the thermal transport in Fe₂VAl thin films

Seongho Choi [●],[1,][*] Satoshi Hiroi,[2] Manabu Inukai,[1] Shunsuke Nishino,[1] Robert Sobota,[1] Dogyun Byeon [●],[1]
Masashi Mikami [●],[3] Masaharu Matsunami,[1] and Tsunehiro Takeuchi [●][1,4,5]

[1]*Toyota Technological Institute, 2-12-1, Hisakata, Tempaku-ku, Nagoya, Aichi 468–8511, Japan*

[2]*National Institute for Materials Science, 1-1-1, Koto, Sayo, Sayo, Hyogo 679–5148, Japan*

[3]*National Institute of Advanced Industrial Science and Technology, 2266-98, Anagahora, Shimoshidami, Moriyama-ku, Nagoya, Aichi 463–8560, Japan*

[4]*CREST, Japan Science and Technology Agency, Tokyo, 102-0076, Japan*

[5]*Institute of Innovation for Future Society, Nagoya University, Nagoya, 464–8603, Japan*

The thermal transport properties of M/Fe₂(V, Ta)Al/M (M = Mo, W) multilayer thin films, which were epitaxially grown on the [100] MgO single-crystal substrates by means of a radio-frequency magnetron sputtering system, were systematically investigated using a picosecond pulsed laser heating time-domain thermoreflectance method. Not only the thermal diffusivity but also the boundary thermal resistance was strongly affected by both the Ta substitution for V in Fe₂VAl and the elements in the metallic layer of top and bottom sides. From the first-principles density-functional theory calculations, we found that such changes in heat transport properties were directly related to the intrinsic phonon dispersion. In the Fe₂(V, Ta)Al layer thickness region of less than 14 nm, the boundary thermal resistances of all thin-film series abruptly decreased with decreasing the thickness, which was due to the coherently ordered interfacial structure.

I. INTRODUCTION

Thermoelectric generators are capable of converting heat to electricity without mechanical components. Their performance is quantified by the dimensionless figure of merit, $zT = S^2\sigma T/(\kappa_e + \kappa_l)$ of thermoelectric materials used in the generators, where S, σ, κ_e, and κ_l represent the Seebeck coefficient, electrical conductivity, electronic and lattice contributions to the total thermal conductivity κ, respectively [1,2]. The electrical factors of S, σ, and κ_e are interdependent one with another due to the charge-carrier dependency, which makes increasing zT extremely difficult. Given a weak correlation between the electrical factors and lattice dynamics, to decrease κ_l would be an effective way to get a high zT.

Among various achievements for the reduction of κ_l, thin-film approaches have notably opened a possibility to reduce κ_l. In particular, the multilayer thin films have enabled quantitative investigation of the grain-size dependence of κ_l as well as the novel phenomena such as zone-folding effect and interface vibrational modes [3–5]. When the thickness of thin films is reduced to nanoscales, the boundary thermal resistance between layers becomes comparable to the thermal resistance of layer-component materials [6,7]. The boundary thermal resistance may become remarkable in the multilayer thin films in which a periodic structure is formed by alternate stacking of nanoscale layers of materials with different crystal structures and different atomic masses [8,9].

A heavy-element partial substitution for materials in multilayer thin films would be one of the most effective methods to reduce κ_l, because it may lead to the impurity scattering and phonon dispersion modulation effects such as the decrease of phonon group velocity and the increase of umklapp process. However, the combined effects of heavy-element substitution and reducing thickness of thin films on the lattice dynamics has not been clarified yet.

Fe₂VAl-based thermoelectric materials of $L2_1$-type full-Heusler phase have been widely investigated as one of the most promising thermoelectric materials. It is, because of their possession of a large power factor ($S^2\sigma$) of more than 6–7 mW m⁻¹ K⁻² near room temperature as well as strong mechanical property, cheap, and nontoxic constituents [10–14]. Takeuchi *et al.* experimentally demonstrated that the κ_l can be reduced without degradation of electrical properties on the basis of the first-principles calculations for heavy transition element substitution in Fe₂VAl [11,12]. Renard *et al.* reported that the substitutions of 5*d* heavy elements such as Ta and W for V in Fe₂VAl significantly decrease κ_l, resulting in the increment of zT by nearly five times [13]. Their electrical resistivity data of Ta-substituted Fe₂VAl showed a weak temperature dependence of 0.4(1) mΩ cm over the temperature range of 300–1200 K rather than showing positive temperature coefficient of electrical resistivity (TCR) that is generally observable in typical metallic materials. The temperature dependence of electrical resistivity of metallic materials is generally determined by the temperature dependence of scattering probability of electrons and energy-dependent electronic structure, and the former is mainly responsible for the positive TCR. Therefore, we considered that the negative

*seonghochoi313@gmail.com

104312-1

TCR at high temperature above 500 K without having an energy gap would be accounted for with the strongest limit known as the Mott-Ioffe-Regel limit [15] and the concave shape of electronic density of states in the vicinity of chemical potential. Most recently, unusually high value of dimensionless figure of merit $zT = 5$ was reported for the Fe_2VAl-based thin-film samples sputtered on undoped Si wafer due to a huge enhancement in the Seebeck coefficient [16]. Hence, it has been expected that combining multilayer thin films onto $5d$-element substituted Fe_2VAl would lead to the increase of zT through the reduction of κ_l without deterioration of electrical properties.

In the present study, we have epitaxially grown three-layer thin films composed of not only heavy-element substituted Fe_2VAl layer of intermediate but also metal (Mo or W) layers both of top and bottom sides on MgO (100) substrates. The thermal properties of as-prepared multilayer thin films were estimated using the picosecond time-domain thermoreflectance technique (TDTR), where the thermal conductivity in the $L2_1$ phase was estimated together with the boundary thermal resistances between the $L2_1$ phase and metal layers. The theoretical calculation based on first-principles density-functional theory was carried out to quantitatively unveil the correlation between intrinsic phonon modes in layer materials consisting of multilayer thin films, which supported the experimental results.

II. METHODS

A. Sample preparation and measurements

$M/Fe_2(V, Ta)Al/M$ (M = Mo, W) thin films were grown on the [100] MgO single-crystal substrates using a radio-frequency magnetron sputtering system (VTR-150F/SRF, Ulvac Kiko, Japan). For the fabrication of thin films, 2-in. target disks of $Fe_2V_{0.92}Ta_{0.08}Al$, Mo, and W were prepared. For the TDTR measurement, Mo layers of 100-nm thickness, which absorbs the pumping laser and also possesses a significant temperature dependence in reflectivity for the probing laser, were deposited at the top and bottom sides of thin films. The sputtering chamber was evacuated below 2.0×10^{-4} Pa before starting a flow of argon gas. During the deposition, the temperature of the substrate was maintained at 873 K, the argon gas pressure at 2.0 Pa, and the rf power at 80 W. The growth rate of samples was determined to be 19 ± 3 nm/min for the $Fe_2(V, Ta)Al$ and Mo layers, and 16 ± 3 nm/min for the W layer, as acquired by synchrotron radiation x-ray reflectivity measurements in the previous work [17]. To confirm the solubility of Ta in the Fe_2VAl, electron probe microanalysis (JXA-8230, JEOL, Japan) was employed at an accelerating voltage 15 kV at 20 locations of $Fe_2(V, Ta)Al$ single-layer thin film with thickness of more than 600 nm deposited on MgO at 873 K and thus, the averaged Ta content was 6.7 ± 0.4 at. % for the V site.

We carried out the out-of-plane x-ray diffraction (XRD) in the cross-plane direction in the range 20°–80° using the Cu $K\alpha$ line ($\lambda = 1.5418$ Å, Bruker D8 ADVANCE) at room temperature. To investigate the roughness effect, the single-layer thin films of Mo, W, and $Fe_2(V, Ta)Al$ were prepared at the same sputtering conditions and measured by atomic force microscopy (AFM, Nano Navi Real/Nano Cute of Seiko

Instruments Inc., Japan). To investigate the cross-plane thermal transport, the picosecond TDTR measurements (PicoTR, PicoTherm Corporation) with a rear-heating front-detection (RF) configuration at room temperature were carried out.

B. Theoretical calculations

The phonon calculations were performed within the framework of the force-constants method. A unit cell and $2 \times 2 \times 2$ superlattices were used for phonon structure calculation (dispersion curves and density of states) in the single-element (Mo and W) and Fe_4VXAl_2 (X = V, Ta) systems. Real-space force constants of the supercell were calculated in the density functional perturbation theory (DFPT) as implemented in the VASP code. The generalized gradient approximation of Perdew, Burke, and Ernzerhof was used for the exchange-correlation potential. A plane-wave energy cutoff of 500 eV was employed in the calculations. The phonon frequencies were computed from the force constants using the PHONOPY code [18]. The phonon density of states were sampled using the $16 \times 16 \times 16$ mesh.

III. RESULTS

A. Crystallographic characterization

Figures 1(a) and 1(b) show the symmetric θ-2θ XRD patterns of $M/Fe_2(V, Ta)Al/M$ (M = Mo, W) thin films. Those two series of samples showed similar patterns for $L2_1$ phase and the similar thickness dependence with the recently reported results of $W/Fe_2VAl/W$ thin films [17]. In the thicker region of more than 14 nm, the $00l$ peaks of $L2_1$ phase and the peak of Mo 002 or W 002 were observed and the intensity of $L2_1$ peaks increased with increasing thickness because of the increasing volume fraction of the relaxed $L2_1$ phase. However, the thin films of less than 8 nm in thickness did not show any $L2_1$ peaks, presumably because of the low volume fraction of $L2_1$ phase.

The thickness dependence of the volume fraction of $L2_1$ phase was confirmed in the reciprocal-space mapping using synchrotron x ray of $Mo/(Fe_2VAl/W)n/Mo$ superlattice thin films; the thinnest superlattice having a period of 1.9 nm showed the strong satellite reflections stemmed from superlattice with highly ordered structure, the superlattice having a period of 3.2 nm displayed no satellite reflection due to the misfit dislocations, and the superlattice having a period of 6.3 nm has recovered a symmetric reflection of $L2_1$ phase due to the relaxed $L2_1$ phase [19]. From these results, one can naturally expect that the crystal structure variation within very thin region of several nanometers in thicknesses is characterized by (i) the coherently strained epitaxial-grown structure free from dislocations. With increasing thickness nearly equal to 3.2 nm, (ii) the structure with misfit dislocations appears at the portion slightly apart from the boundaries between $L2_1$ layer and metal layer. With further increasing the thickness, (iii) the relaxed $L2_1$ phase forms after (ii). The samples were classified into two groups by their component structures (i)–(iii). The first group involves the samples of less than 8 nm in thickness. The samples of this group have (i) misfit dislocations and (ii) homogeneously strained, well-ordered structures near interfaces. The second group involves samples of more than 14 nm
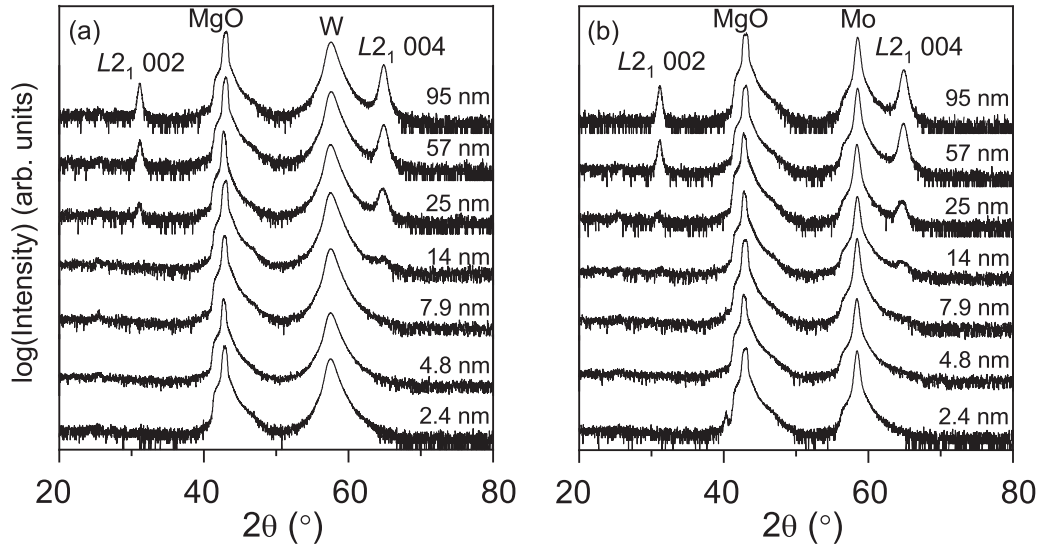
FIG. 1. Symmetric θ-2θ x-ray diffraction patterns of cross-section direction for (a) Mo/Fe$_2$(V, Ta)Al/Mo and (b) W/Fe$_2$(V, Ta)Al/W thin films with varying thickness of Fe$_2$(V, Ta)Al layer at room temperature.

in thickness. These samples consist mainly of (iii) the relaxed $L2_1$ phase and have also both (i) misfit dislocations and (ii) partially strained structure persisting near the interfaces. Such features should have strong effects on the phonon propagation.

B. Thermal transport analysis of thin films

M/Fe$_2$(V, Ta)Al/M ($M =$ Mo, W) thin films were measured by means of the TDTR method. The thermal transport property was estimated via two steps of the single- and three-layer analyses for the three-layer thin films, in which the three-layer analysis provides us the solution for multilayer thin films that cannot be measured as a single layer because of the low sensitivity to temperature detection.

1. Single-layer model analysis

Figures 2(a) and 2(b) show the transient curves of temperature obtained from TDTR measurements using the

rear-heating and front-detection (RF) configuration. According to an analysis solution for a single-layer thin film developed by Baba *et al.*, in the RF configuration, the temperature at the front surface of a single-layer thin film under the adiabatic condition by heat loss into the substrate is given as follows [20,21]:

$$
\begin{aligned}
T(t) = \frac{\Delta T d}{l} \sum_{n=-\infty}^{\infty} \Bigg\{ & \gamma^{|n|} \exp\left[-\frac{(2n-1)^2 h^2}{4} \right] \\
& \times \exp\left[\left(\frac{(2n-1)h}{2} + \frac{d}{lh} \right)^2 \right] \\
& \times \mathrm{erfc}\left[\left(\frac{(2n-1)h}{2} + \frac{d}{lh} \right) \right] \Bigg\},
\end{aligned}
\tag{1}
$$

where ΔT, d, and l are the equilibrium temperature rise for the film to the substrate, the total thickness of the single-layer
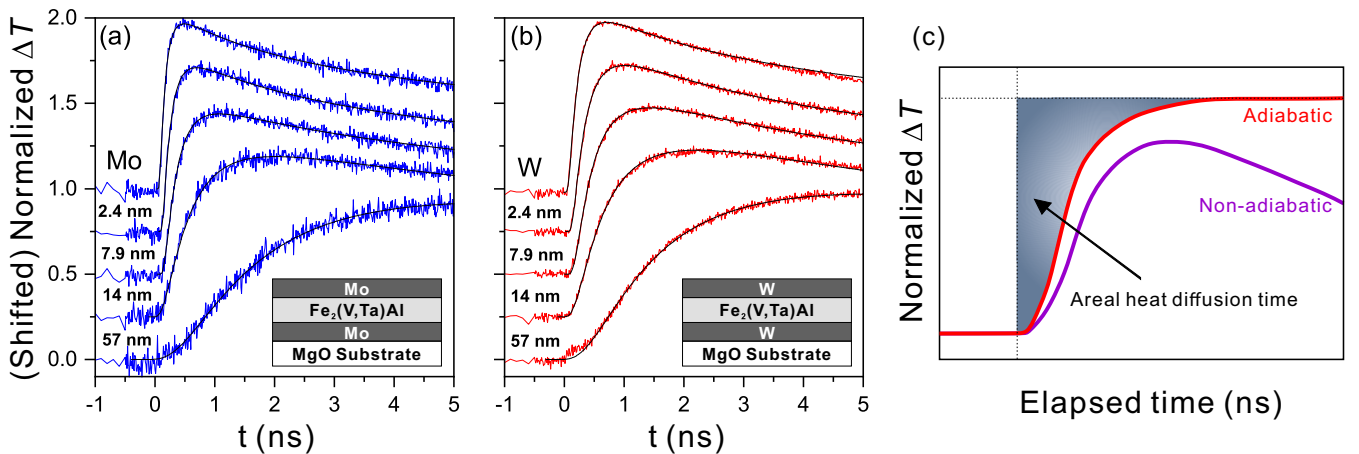

FIG. 2. Time dependence of thermoreflectance signal curves with fitting results, as marked by black lines obtained from Eq. (1) for (a) Mo/Fe$_2$(V, Ta)Al/Mo and (b) W/Fe$_2$(V, Ta)Al/W thin films with various thickness of Fe$_2$(V, Ta)Al layer at room temperature. (c) The definition of the areal heat diffusion time drawn as shaded region.

TABLE I. γ values for three-layer thin films obtained by fitting Eq. (1).

Thickness of $L2_1$ layer (nm)	Mo/Fe$_2$(V, Ta)Al/Mo	W/Fe$_2$(V, Ta)Al/W
1.4	0.3880	0.2123
2.4	0.3704	0.1919
4.8	0.3299	0.1582
7.9	0.3080	0.0969
14	0.0960	−0.0782
25	0.0863	−0.1120
38	0.0399	−0.1670
57	−0.2021	−0.1513
95	−0.4584	−0.0410

thin film, and the penetration depth into Mo (24.5 nm) and W (21.3 nm) of pulse laser with the wavelength of 1550 nm used for heating, respectively [22]. In this analysis, one can regard the $L2_1$ layer and top/bottom metal layers as a single-layer thin film. The h is a dimensionless term defined as $h = \sqrt{\tau/t}$, where τ and t is the heat diffusion time and the delay time, respectively. Another dimensionless term γ corresponding to the magnitude of heat loss at the propagation into substrate was obtained by fitting using Eq. (1) and listed in Table I. The γ can be expressed by the following equation:

$$\gamma = \frac{b_f - b_s}{b_f + b_s}, \qquad (2)$$

where b_f and b_s are the thermal effusivities of the film and the substrate, respectively. The erfc(x) is the complementary error function defined as the following equation:

$$\mathrm{erfc}(x) = \frac{2}{\sqrt{\pi}} \int_x^\infty \exp(-F^2)dF, \qquad (3)$$

The fitting results with Eq. (1) are shown with the measured data in Figs. 2(a) and 2(b), where the blue and red curves indicate the transient temperature curves. According to Baba *et al.* [21], the areal heat diffusion time, A, can be defined as $A = \tau/6$, for a single-layer film under adiabatic condition, where the definition of A was shown in Fig. 2(c).

However, in the nonadiabatic case, as shown in Fig. 2, the temperature rises after the zero time and decreases after the maximum rise. Figures 2(a) and 2(b) showed that all samples were the nonadiabatic, where the magnitude of samples with $L2_1$ layer of 57 nm had a maximum around 6 ns and then decreased to 50 ns with increasing delay time. The fact means that it is necessary to correct such an unfavorable negative slope. Hence, if assuming no radiation heat, the decreasing behavior after the maximum would be due to the heat effusion from the thin-film sample into the MgO substrate, which was corrected by the fitting parameter γ.

As shown in Eqs. (1) and (2), the nature of the thermoreflectance signal is a function of not only the thermal diffusivity of the film but also the thermal effusivity from the film to the substrates. The thermal effusivity means an ability to exchange thermal energy with its surroundings and is defined as $b = \sqrt{\kappa c \rho}$, where κ, c, and ρ are the thermal conductivity, the specific heat, and the density, respectively. The MgO single-crystalline substrate that we used in this work has the relatively high thermal conductivity ($>37\,\mathrm{W\,m^{-1}\,K^{-1}}$) as well

as higher volumetric heat capacity ($\sim3.3 \times 10^6\,\mathrm{J\,m^{-3}\,K^{-1}}$) than materials [Mo, W, Fe$_2$VAl, Fe$_2$(V, Ta)Al] in our thin-film samples, which indicates that the substrate has the high thermal effusivity. In other words, in our thin-film samples, since the thermal energy can easily move from the film to substrate, it can be taken in not adiabatic condition but nonadiabatic condition. The thermoreflectance signals in Figs. 2(a) and 2(b) definitely show to be in nonadiabatic condition as a negative slope.

The γ can be of the values from −1 to 1, in which γ would be close to 1 when $b_f \gg b_s$, γ would be zero when $b_f = b_s$, and γ would be close to −1 when $b_f \ll b_s$ as shown in Eq. (2). Table I shows the γ decreased with increasing the volume fraction of $L2_1$ layer, which would be due to the relatively small effusivity of $L2_1$ layer. Furthermore, the γ appeared as the values of different range as the metal layer. This caused the the sign change of the γ values at a different $L2_1$ thickness, which is mainly attributed to the different thermal diffusivity between Mo and W because their heat capacity values are very similar with each other.

By using the obtained parameters, we calculated the areal heat diffusion time by assuming M/Fe$_2$(V, Ta)Al/M to be a single layer.

2. Three-layer decomposition approach for a single-layer model

For the areal heat diffusion time obtained from a single-layer model, when it is assumed that the metal layers of top and bottom sides are the same composition and thickness as each other, the contributions of thermal resistance in each layer can be separated by the following equation [17,21,23]:

$$A = \frac{\frac{\left(\frac{4}{3}+\Gamma\right)d_M^2}{\alpha_M} + \frac{\left(\frac{1}{\Gamma}+1+\Gamma/6\right)d_{L2_1}^2}{\alpha_{L2_1}}}{2+\Gamma} + 2RC_Md_M\frac{1+\Gamma}{2+\Gamma}. \qquad (4)$$

Here d, α, and R represent the thickness, the thermal diffusivity of each layer, and the boundary thermal resistance between $L2_1$ phase and metal layers, respectively. Γ is the ratio of the heat capacity of the $L2_1$ phase layer to that of the metal layer, and is described by the following relation:

$$\Gamma = \frac{C_{L2_1}d_{L2_1}}{C_Md_M}, \qquad (5)$$

where C values present the heat capacity per unit volume of each layer. The values of C and α of Mo, W, and Fe$_2$(V, Ta)Al were thus determined and summarized in Table II.

TABLE II. Heat capacity per unit volume C and thermal diffusivity α for Mo, W, and Fe$_2$(V, Ta)Al bulk samples at room temperature.

Samples	$C(\times 10^6 \text{J m}^{-3}\text{K}^{-1})$	$\alpha(\times 10^{-5}\text{m}^2 \text{ s}^{-1})$
Mo	2.55	4.63
W [17]	2.58	2.19
Fe$_2$(V, Ta)Al	2.75	0.31

Figure 3 shows $L2_1$ phase layer thickness dependence of areal heat diffusion time A for Mo/Fe$_2$(V, Ta)Al/Mo, W/Fe$_2$(V, Ta)Al/W, and W/Fe$_2$VAl/W [17] thin films obtained at room temperature. The data of each series of samples definitely showed different thickness dependence below and above 14 nm. Therefore, we decided to firstly fit only the data staying above 14 nm using Eq. (4). The used parameters are the thermal diffusivity of $L2_1$ phase α_{L2_1} and the boundary thermal resistance R. The resulting values are summarized in Table III. Noting here that the α_{L2_1} mainly determines the slope of the fitting curves while R represents the value at the zero thickness ($D = 0$). The α_{L2_1} values of Ta doping samples (red colored data) were lower than that of the nondoped one, which would be attributed to impurity scattering of phonons. The slope of the data, which represents α_{L2_1} values, became different when the metal layer was different. This fact means that the difference in phonon dispersion in the metal layer Mo or W would greatly affect α_{L2_1} most likely because of the difference in phonon mode matching between metals and $L2_1$ phase.

Another important factor is the variation of boundary resistance R in association with the large lattice mismatches between the $L2_1$ phase and metal layers. This degree of mismatch would produce lattice stress near the interfaces and dislocations consequently. The lattice mismatch $\Delta a/a_M$ of W/Fe$_2$VAl/W is 0.098, whereas it reduces to 0.092 and 0.079 in W/Fe$_2$(V, Ta)Al/W and Mo/Fe$_2$(V, Ta)Al/Mo, respectively. In good consistency with the smallest value of lattice mismatch, Mo/Fe$_2$(V, Ta)Al/Mo possessed the smallest interlayer boundary thermal resistance R. The fact that the value of R increases with increasing $\Delta a/a_M$ definitely indicates that the interlayer boundary thermal resistance is strongly affected by the strain, stress, and consequently introduced dislocations. More discussion about the phonon modulation effects for the α_{L2_1} and the R values are given in Sec. IV.

In the small $L2_1$ thickness region of less than 14 nm, A values of all three-layer thin films shown in Fig. 3 came to possess a similar thickness dependence. Such similar slopes of all series in that thin region may indicate the similar thermal diffusivity in $L2_1$ layer to one another, because the slope in
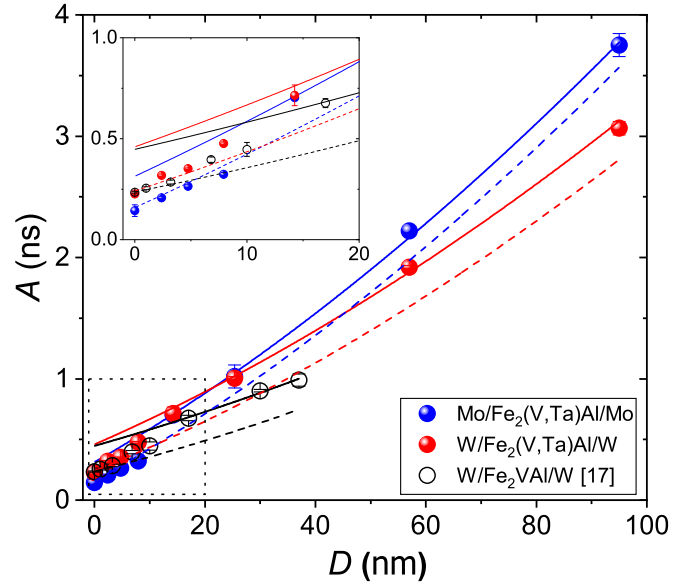

FIG. 3. $L2_1$ phase layer thickness (D) dependence of areal heat diffusion time (A) of Mo/Fe$_2$(V, Ta)Al/Mo, W/Fe$_2$(V, Ta)Al/W, and W/Fe$_2$VAl/W [17] thin films at room temperature. The solid curves indicate fitting results of Eq. (4) for all data above 14 nm in $L2_1$ phase layer thicknesses and the dashed curves indicate fitting results using $R = 0$ for all data.

the fitting using Eq. (4) is dominantly attributed to the thermal diffusivity of $L2_1$ layer. This possibly means that, in this thin region, the interference effect for phonon propagation by Ta substitution for V site in $L2_1$ layer became significantly weakened due to the significantly strained structure. On the other hand, one may think that such abrupt changes of behavior in thickness dependence of A might be due to the contact between top and bottom metal layers in association with elemental mixing and/or formation of holes in an intermediate layer [24,25]. However, we confirmed both from x-ray reflectivity and the high-resolution transmission microscopy that our thin-film samples are free from the interlayer contact [17,19], and therefore it must be attributed to the intrinsic nature of thin films.

Notably, the A values of all samples fell on the dashed curve obtained with an assumption of $R = 0$. Such abrupt reductions of R values in the thickness region of less than 14 nm would be directly related to the strained structure including the coherently arranged structure having almost no dislocation. In such coherent structure near the interlayer boundaries, phonons could pass through without being scattered. Such structural and thermal features would have a close relation with the coherent-incoherent crossover of phonon conduction

TABLE III. Thermal diffusivity α_{L21}, boundary thermal resistance R, and lattice mismatch $\Delta a/a_M$ of Mo/Fe$_2$(V, Ta)Al/Mo, W/Fe$_2$(V, Ta)Al/W, and W/Fe$_2$VAl/W thin film samples at room temperature. α_{L21} and R values were obtained by fitting Eq. (4).

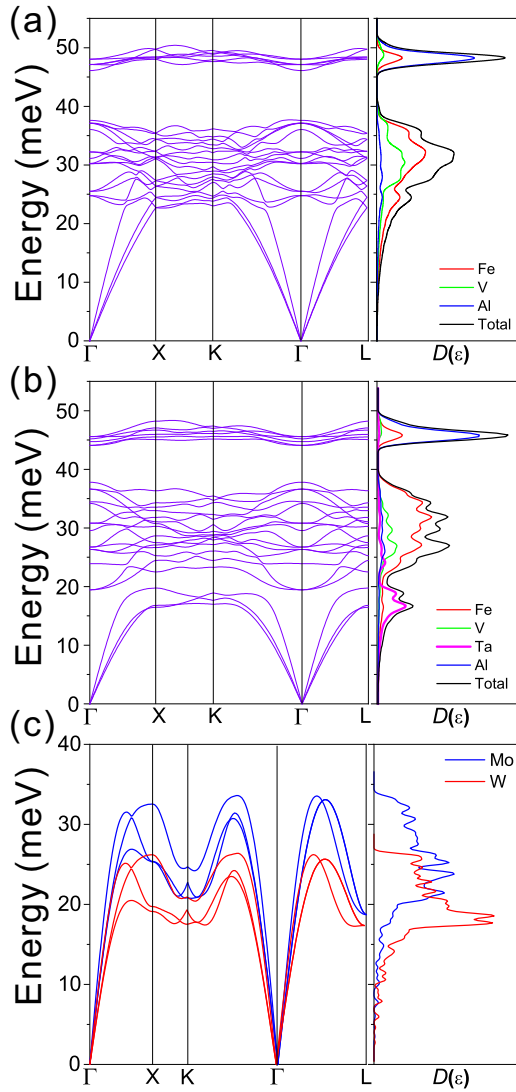| Samples	$\alpha_{L21}(\times 10^{-6} \text{ m}^2/\text{s})$	$R(\times 10^{-10} \text{ m}^2 \text{ K/W})$	$\Delta a/a_M(\%)$
Mo/Fe$_2$(V, Ta)Al/Mo	2.1 ± 0.1	2.6 ± 1.1	7.9
W/Fe$_2$(V, Ta)Al/W	2.4 ± 0.1	7.2 ± 1.8	9.2
W/Fe$_2$VAl/W [17]	3.4 ± 0.4	6.6 ± 1.6	9.8

FIG. 4. Phonon dispersion curves and phonon density of states (VDOS) of (a) $Fe_4V_2Al_2$, (b) Fe_4VTaAl_2, and (c) Mo and W.

through the interlayer boundaries [26,27]. In particular, the perfect consistency of $Mo/Fe_2(V, Ta)Al/Mo$ for the dashed fitting curves assuming $R = 0$ might result from the coherent interfacial structures in association with the small lattice mismatch.

IV. DISCUSSION

In order to gain deeper insight into the experimental results, we calculated the phonon dispersions and vibrational density of states.

Figures 4(a) and 4(b) show the phonon dispersion and vibrational density of states (VDOS) of $Fe_4V_2Al_2$ and Fe_4VTaAl_2 calculated on the basis of the harmonic interatomic force constants. All the phonon frequencies are positive, which indicates that the structures models of $Fe_4V_2Al_2$ and Fe_4VTaAl_2 are dynamically stable.

The substitution of V by Ta induced some remarkable changes in phonon dispersion. The most pronounced variation is observed in the sound velocity in acoustic branches. The

calculated sound velocities close to Γ for the TA/TA′/LA/ (average) acoustic modes are 4.54/5.04/7.88/(5.26) km s^{-1} for $Fe_4V_2Al_2$ and 4.18/4.63/7.12/(4.83) km s^{-1} for Fe_4VTaAl_2. Notably, the values of $Fe_4V_2Al_2$ are close to those in the previously reported paper [28]. The 8.2% reduction of group velocity in Fe_4VTaAl_2 from that of $Fe_4V_2Al_2$ would be naturally related with a decrease in the lattice thermal conductivity in Fe_4VTaAl_2. Another distinct variation in the phonon branches is the energy of optical branches. Those of Fe_4VTaAl_2 significantly decreased, e.g., the lowest-energy branches at *X-K* line move from ∼23 meV of $Fe_4V_2Al_2$ to ∼17 meV of Fe_4VTaAl_2. This variation in phonon branches resulted in the presence of shallow peaks at ∼17 meV in the VDOS for Fe_4VTaAl_2. It should be also emphasized that Ta substitution would have contributed to a significant increase in umklapp process of phonon scattering, because of the large number of excitation of phonons near the zone boundary. As another strong evidence, this is well in agreement with the inelastic x-ray scattering spectra for single crystal of $Fe_2V_{0.95}Ta_{0.05}Al$ recently reported by Kimura *et al.*, which also showed the additional modes at around 17 meV by Ta substitution [28,29]. Therefore, it is safely argued that Ta partial substitution for V in Fe_2VAl contributes to both the reduction of sound velocity and the enhancement of umklapp processes of phonon scattering, leading to the significant reduction of lattice thermal conductivity.

In the next step, we need to consider the feature of the phonon propagation related to Mo or W layers, as it would affect the transmission probability of phonons across interfaces between the $L2_1$ phase and metal layer.

Figure 4(c) shows the phonon band structures for Mo and W obtained from theoretical calculations. The highest energy of phonon of W is located at 10 meV lower than that of Mo because the atomic mass of W is nearly 2 times larger than Mo. In order to know the VDOS matching between $L2_1$ phase and bcc metals, the combined VODS, $D_{L2_1-M}(\varepsilon)$, were calculated using the following formula:

$$D_{L2_1-M}(\varepsilon) = f_{BE}(\varepsilon)D_{L2_1}(\varepsilon)D_M(\varepsilon), \quad (6)$$

where $f_{BE}(\varepsilon) = 1/(e^{\hbar\omega/k_BT} - 1)$ is the Bose-Einstein distribution function at 300 K, and $D_{L2_1}(\varepsilon)$ and $D_M(\varepsilon)$ are the VDOS of $L2_1$ phase and metal layers, respectively. The resulting $D_{L2_1-M}(\varepsilon)$ shown in Fig. 5 provided us with information about probability of elastic phonon transfer across the interlayer boundaries.

As shown in Fig. 5, $D_{L2_1-W}(\varepsilon)$ possesses larger magnitude than $D_{L2_1-Mo}(\varepsilon)$ at lower energies below 20 meV because of the heavier mass of W. Thus, the probability of the lower-energy phonons of higher group velocity passing through the interlayer boundaries would be higher in the $L2_1$/W boundaries than $L2_1$/Mo boundaries. This might be the reason why W/Fe$_2$(V, Ta)Al/W possesses the slightly larger α_{L2_1} value than Mo/Fe$_2$(V, Ta)Al/Mo in the $L2_1$ thickness region of more than 14 nm as shown in Table II.

On the other hand, the number of phonons is related with the phonon transmission probability across the interlayer boundaries. Hence, the phonon mode matching between $L2_1$ layer and metal layer would be directly correlated to the boundary thermal resistance in interlayer boundaries. Here, we found out that the ratio of the boundary thermal
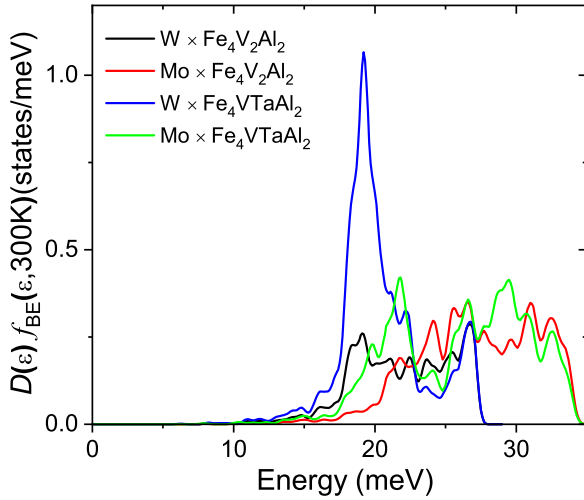
FIG. 5. Transmission probability of VDOS products between $(Fe_4V_2Al_2, Fe_4VTaAl_2)$ and (Mo, W).

resistance of $Mo/Fe_2(V, Ta)Al/Mo$ to that of $W/Fe_2(V, Ta)Al/W$ was approximately 0.36 and the ratio of $D_{Fe_4VTaAl_2-W}(\varepsilon)$ to $D_{Fe_4VTaAl_2-Mo}(\varepsilon)$ was approximately 0.93. We can consider that the large difference between those values would have stemmed from the lattice mismatch difference between $Mo/Fe_2(V, Ta)Al/Mo$ and $W/Fe_2(V, Ta)Al/W$, because the theoretical calculation did not include any condition related to the physical imperfections in interfaces.

However, to concretely confirm these arguments, it should be necessary to additionally carry out the systematic study including the different metals with the small lattice mismatching to remove the effects of interfacial roughness and defects.

Another important factor to affect the propagation of phonons is a roughness at the interlayer boundaries. Therefore, we prepared monolayer thin films of Mo, W, and $Fe_2(V, Ta)Al$ having thicknesses of $\sim$95, $\sim$89, and $\sim$95 nm, respectively/correspondingly, and performed atomic force microscope measurements for those thin films as shown in Fig. 6. The AFM images display that Mo and $Fe_2(V, Ta)Al$ thin films are quite rough compared to W thin film. The rms roughness of Mo, W, and $Fe_2(V, Ta)Al$ thin films were 0.61 ± 0.10 nm, 0.19 ± 0.03 nm, and 0.76 ± 0.09 nm, respectively. Even though the rms of Mo was three times larger than that of W, the boundary thermal resistance of the thin film with Mo layers was much smaller than those of thin films with W layers as shown in Table III. Thus, one can expect that the effect

of interfacial roughness for phonon propagation is negligible and the lattice mismatch between $L2_1$ and metal layer was dominant for boundary thermal resistance.

As a result, in this work, we found four critical points that affect lattice thermal conductivity of the present samples.

(i) The $5d$ heavy-element substitution for $L2_1$-type Fe_2VAl effectively reduced the thermal diffusivity by simultaneously inducing the reduction of phonon group velocity and the remarkably enhanced umklapp processes as well as impurity scattering.

(ii) Additional reduction of thermal diffusivity in $Mo/Fe_2(V, Ta)Al/Mo$ could be acquired from the VDOS mismatching between $L2_1$ phases and metals.

(iii) In the $L2_1$ thickness region of more than 14 nm, the smallest lattice mismatch of $Mo/Fe_2(V, Ta)Al/Mo$ directly contributed to the reduction of boundary thermal resistance.

(iv) In the $L2_1$ thickness region of less than 14 nm, the boundary thermal resistances of all samples abruptly decreased with decreasing of the thickness of $L2_1$ layer, which would be due to the coherently strained but highly ordered lattice near the interfaces.

We make comments on the possible performance of Fe_2VAl-based thermoelectric materials using the data obtained in this study. We experimentally got the thermal diffusivity of 2.1×10^{-6} m^2/s for the $L2_1$ layer in $Mo/Fe_2(V, Ta)Al/Mo$ at room temperature. With this value and the power factor of 6.0 of 6.0 Wm^{-1} K^{-2} of Ta-doped Fe_2VAl bulk sample [13] at room temperature, we estimated both the thermal conductivity and the dimensionless figure of merit to be $k = 5.8$ Wm^{-1} K^{-1} and $zT = 0.31$, respectively. The magnitude of zT is nearly two times larger than that of the previously reported $zT = 0.17$ for Ta-doped Fe_2VAl [13] at room temperature.

From the experimental and theoretical results obtained in this study, we are convinced that the combination of a heavy-element substitution and boundary scattering modifications can be a strategy generally usable for efficient performance enhancements of thermoelectric materials.

V. CONCLUSION

We investigated the cross-plane component of thermal diffusivity in $Fe_2(V, Ta)Al$ layer to get an insight for the thermal transport effect by $5d$ heavy-element substitution into Fe_2VAl-based thin films. The boundary thermal resistance between the $L2_1$ phase and metal layers was also investigated

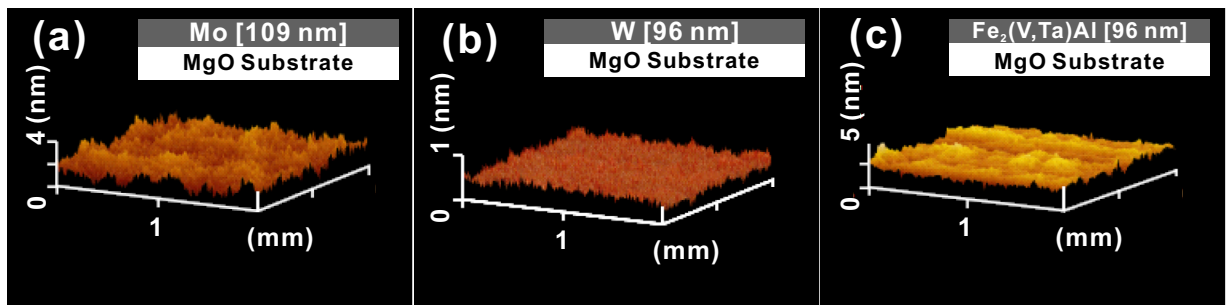FIG. 6. AFM images for single-layer thin films of (a) Mo, (b) W, and (c) $Fe_2(V, Ta)Al$ deposited on MgO substrate at 873 K.

in detail. The partial substitution of Ta for V in Fe$_2$VAl definitely decreased the thermal diffusivity by (a) the remarkable increase of umklapp processes of phonon scattering caused by lowering of energy of optical phonon branches together with (b) the reduction of group velocity of acoustic phonons. The samples containing W layers led to the reduction of more than 10% in the thermal diffusivity of the $L2_1$ phase from the value observed for the samples containing Mo layers due to the lowering of optical phonon branches and the group velocity of acoustic phonons. We also figured out that the phonon transmission probability between the $L2_1$ phase and metal layer may affect the thermal conductivity of the multilayered samples. Surprisingly, in the samples containing the $L2_1$ phase

thinner than 14 nm, the boundary thermal resistance abruptly decreased presumably because the coherent interfacial structure having no dislocations was formed in the vicinity of interlayer boundaries. It is considered that such coherent interlayer boundaries allow the phonons to pass through without being scattered.

[1] Y. Kawaharada, K. Kurosaki, and S. Yamanaka, J. Alloys Compd. **349**, 37 (2003).

[2] M. Mikami, M. Inukai, H. Miyazaki, and Y. Nishino, J. Electron. Mater. **45**, 1284 (2016).

[3] C. Colvard, R. Merlin, M. V. Klein, and A. C. Gossard, Phys. Rev. Lett. **45**, 298 (1980).

[4] A. K. Sood, J. Menéndez, M. Cardona, and K. Ploog, Phys. Rev. Lett. **54**, 2111 (1985).

[5] A. K. Sood, J. Menéndez, M. Cardona, and K. Ploog, Phys. Rev. Lett. **54**, 2115 (1985).

[6] S.-M. Lee and D. G. Cahill, J. Appl. Phys. **81**, 2590 (1997).

[7] R. J. Stoner and H. J. Maris, Phys. Rev. B **48**, 16373 (1993).

[8] X. Ran, Y. Guo, Z. Hu, and M. Wang, Front. Energy Res. **6**, 28 (2018).

[9] M. Nomura, J. Shiomi, T. Shiga, and R. Anufriev, Jpn. J. Appl. Phys. **57**, 080101 (2018).

[10] Y. Feng, J. Y. Rhee, T. A. Wiener, D. W. Lynch, B. E. Hubbard, A. J. Sievers, D. L. Schlagel, T. A. Lograsso, and L. L. Miller, Phys. Rev. B **63**, 165109 (2001).

[11] T. Takeuchi, Y. Terazawa, Y. Furuta, A. Yamamoto, and M. Mikami, J. Electron. Mater. **42**, 2084 (2013).

[12] Y. Terazawa, M. Mikami, T. Itoh, and T. Takeuchi, J. Electron. Mater. **41**, 1348 (2012).

[13] K. Renard, A. Mori, Y. Yamada, S. Tanaka, H. Miyazaki, and Y. Nishino, J. Appl. Phys. **115**, 033707 (2014).

[14] H. Miyazaki, S. Tanaka, N. Ide, K. Soda, and Y. Nishino, Mater. Res. Express **1**, 015901 (2013).

[15] A. F. Ioffe and A. R. Regel, Prog. Semicond. **4**, 237 (1960).

[16] B. Hinterleitner, I. Knapp, M. Poneder, Y. Shi, H. Müller, G. Eguchi, C. Eisenmenger-Sittner, M. Stöger-Pollach, Y. Kakefuda, N. Kawamoto, Q. Guo, T. Baba, T. Mori, S. Ullah, X. Q. Chen, and E. Bauer, Nature (London) **576**, 85 (2019).

[17] S. Hiroi, S. Choi, S. Nishino, O. Seo, Y. Chen, O. Sakata, and T. Takeuchi, J. Electron. Mater. **47**, 3113 (2017).

[18] A. Togo, L. Chaput, and I. Tanaka, Phys. Rev. B **91**, 094306 (2015).

[19] S. Hiroi, S. Nishino, S. Choi, O. Seo, J. Kim, Y. Chen, C. Song, A. Tayal, O. Sakata, and T. Takeuchi, J. Appl. Phys. **125**, 225101 (2019).

[20] N. Taketoshi, T. Baba, and A. Ono, Meas. Sci. Technol. **12**, 2064 (2001).

[21] T. Baba, Jpn. J. Appl. Phys. **48**, 05EB04 (2009).

[22] Thermophysical Properties Database System, http://tpds.db. aist.go.jp/tpds-web/index.aspx.

[23] Y. Yamashita, T. Yagi, and T. Baba, Jpn. J. Appl. Phys. **50**, 11RH03 (2011).

[24] N. Oka, R. Arisawa, A. Miyamura, Y. Sato, T. Yagi, N. Taketoshi, T. Baba, and Y. Shigesato, Thin Solid Films **518**, 3119 (2010).

[25] S. Kawasaki, Y. Yamashita, N. Oka, T. Yagi, J. Jia, N. Taketoshi, T. Baba, and Y. Shigesato, Jpn. J. Appl. Phys. **52**, 065802 (2013).

[26] R. Venkatasubramanian, Phys. Rev. B **61**, 3091 (2000).

[27] J. Ravichandran, A. K. Yadav, R. Cheaito, P. B. Rossen, A. Soukiassian, S. J. Suresha, J. C. Duda, B. M. Foley, C. H. Lee, Y. Zhu, A. W. Lichtenberger, J. E. Moore, D. A. Muller, D. G. Schlom, P. E. Hopkins, A. Majumdar, R. Ramesh, and M. A. Zurbuchen, Nat. Mater. **13**, 168 (2014).

[28] V. Kanchana, G. Vaitheeswaran, Y. Ma, Y. Xie, A. Svane, and O. Eriksson, Phys. Rev. B **80**, 125108 (2009).

[29] K. Kimura, K. Yamamoto, K. Hayashi, S. Tsutsui, N. Happo, S. Yamazoe, H. Miyazaki, S. Nakagami, J. R. Stellhorn, S. Hosokawa, T. Matsushita, H. Tajiri, A. K. R. Ang, and Y. Nishino, Phys. Rev. B **101**, 024302 (2020).